Journal of Inorganic Biochemistry 278 (2026) 113262

Contents lists available at ScienceDirect

Journal of Inorganic Biochemistry

journal homepage: www.elsevier.com/locate/jinorgbio

Secondary amide derivatives of Fe(III)-CDTA: Impact of ligand substitution on relaxivity, stability, and kinetic inertness

M. Ludovica Macchia [a], Marco Ricci [b], Mariangela Boccalon [c], Zsolt Baranyai [c,*], Beatrice Ghezzi [b], Valentina Audrito [b], Mauro Botta [b,d,**]

[a] Dipartimento di Scienze Chimiche, Università di Padova, via Marzolo 1, 35131 Padua, Italy
[b] Dipartimento di Scienze e Innovazione Tecnologica Università del Piemonte Orientale, Viale T. Michel 11, Alessandria 15121, Italy
[c] CRB Trieste, Bracco Imaging SpA, AREA Science Park, 34149 Basovizza, TS, Italy
[d] Magnetic Resonance Platform (PRISMA-UPO), Università del Piemonte Orientale, Alessandria, Italy

ARTICLE INFO

Keywords:
Iron(III)
CDTA
MRI
Contrast agents
Relaxivity
Stability

ABSTRACT

The substitution of carboxylate donors with neutral amide groups is a well-established approach for tuning charge distribution and hydration properties in metal chelates; however, its influence on Fe(III) systems has remained largely unexplored. Here, we report two CDTA-derived ligands incorporating one or two secondary butylamide substituents (CD3A-BA and CD2A-BA_2) and comprehensively characterize their Fe(III) complexes using potentiometry, capillary zone electrophoresis, UV–Vis spectrophotometry, transchelation assays (with HBED and human serum transferrin), ^{1}H NMRD, variable-temperature ^{17}O NMR, and in vitro cytotoxicity tests. Amide incorporation decreases ligand basicity and leads to reduced complex stability and kinetic inertness compared to the parent CDTA framework. Nevertheless, the new Fe(III) complexes retain strong metal affinity and remain monohydrated under physiologically relevant conditions. Progressive amide substitution systematically slows inner-sphere water exchange, consistent with the higher residual positive charge of the complexes. Despite this, relaxivity in media mimicking physiological conditions remains unchanged, with negligible protein binding and no detectable Fe(III) release. Cellular assays confirm an absence of cytotoxicity at the tested concentrations. Collectively, these findings elucidate how secondary-amide substitution governs stability, reactivity, and hydration dynamics in Fe(III)–CDTA derivatives, offering valuable insights for the rational design of Fe(III)-based MRI contrast agents.

1. Introduction

Gadolinium-based contrast agents (GBCAs) are among the most widely used diagnostic tools in Magnetic Resonance Imaging (MRI), playing a pivotal role in enhancing image contrast and improving diagnostic accuracy. Currently, more than 40 million GBCA-enhanced MRI examinations are performed worldwide each year [1], underscoring their central role in clinical practice. Over the past several decades, an extensive family of Gd(III) chelates has been synthesized and systematically studied. This collective effort has yielded a profound understanding of the key factors that control their performance, particularly the relationships between the molecular structure of the complex, its dynamic behavior in aqueous solution, and its ability to enhance proton relaxation rates. [2,3] At the same time, rigorous optimization of ligand design has ensured exceptional thermodynamic stability and kinetic inertness, both essential to prevent the release of free Gd(III) ions and to guarantee patient safety. [4,5] Such structure–function insights have established Gd(III) complexes as a benchmark for MRI contrast agent design and continue to serve as a reference for the development of next-generation, metal-based probes with improved efficacy and safety profiles.

However, the widespread use of GBCAs has raised growing concerns about their clinical and environmental impact. Although these complexes are designed to exhibit high thermodynamic and kinetic stability, this same stability limits their natural degradation, leading to environmental persistence and gradual accumulation. Conventional wastewater treatment processes are largely ineffective at removing GBCAs, and as a result, anthropogenic gadolinium is now routinely detected in rivers,

* Corresponding *author*.
** Corresponding *author* at: Dipartimento di Scienze e Innovazione Tecnologica Università del Piemonte Orientale, Viale T. Michel 11, Alessandria 15121, Italy.
E-mail addresses: Zsolt.Baranyai@bracco.com (Z. Baranyai), mauro.botta@uniupo.it (M. Botta).

https://doi.org/10.1016/j.jinorgbio.2026.113262
Received 19 December 2025; Received in revised form 27 January 2026; Accepted 9 February 2026
Available online 10 February 2026

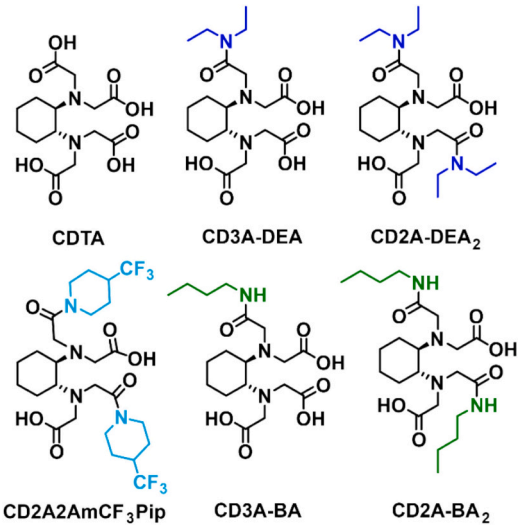

Scheme 1. Chemical structure of the CDTA ligand and its mono- and bis-amide derivatives discussed in the text.

lakes, and even coastal waters, particularly downstream of densely populated areas. [6–8] With global MRI utilization continuing to rise, the development of alternative contrast agents with reduced environmental footprint has become increasingly urgent. In this context, complexes based on endogenous metals such as Fe(III) and Mn(II) are attracting considerable attention as promising, Gd-free substitutes. [9–12] Iron(III)-based systems, in particular, offer the potential to combine efficient T_1 contrast with improved biocompatibility and reduced ecological risk. [13,14] However, designing effective Fe(III)-based contrast agents poses specific challenges.

The ideal ligand must provide not only high thermodynamic stability and kinetic inertness but also efficient contrast enhancement, which is largely determined by the hydration state (q) of the complex. Non-hydrated complexes generally exhibit superior stability; however, their contrast performance is significantly lower. [15] In contrast, hydrated species ($q = 1$) offer enhanced relaxivity but require careful assessment of their stability and redox behavior, as these factors are critical for minimizing potential toxicity. [16,17] Additionally, the overall charge of the complex is an important parameter that must be optimized to achieve favorable biodistribution and excretion. Highly charged complexes may necessitate the use of counterions, which can increase osmolality and potentially elevate toxicity.

One of the most effective strategies in the design of Gd(III) chelates has involved replacing carboxylate groups with amide functionalities, particularly in the context of preclinical studies using nanosized probes. This approach exploits the ease of introducing reactive substituents on the amide nitrogen, enabling the preparation of bifunctional ligands whose complexes can be covalently linked to targeting biomolecules. [18] This modification neutralizes the overall charge and improves biocompatibility, while also affecting the water exchange rate of the complex. [19,20] Although the coordination behavior and relaxometric properties of amide-containing Gd(III) chelates are now well established, considerably less information is available for their Fe(III) analogues. [21,22] In this context, we recently investigated mono- and bis-diethylamide derivatives derived from the CDTA ligand (2,2′,2″,2‴-(((1*S*,2*S*)-cyclohexane-1,2-diyl)bis(azanetriyl))tetraacetic acid, Scheme 1), which represents a promising scaffold for the development of Fe(III) chelates as paramagnetic probes for MRI applications. The CDTA framework enables systematic tuning of key molecular parameters - including hydration state, overall charge, and coordination environment - while preserving favorable relaxometric efficiency and complex stability. [23] Moreover, recently a novel Fe(III) complex based on the CDTA scaffold, namely $[Fe(CD2A2AmCF3Pip)]^+$ (2,2′-(((1*R*,2*R*)-cyclohexane-1,2-diyl)bis((2-oxo-2-(4-(trifluoromethyl)piperidin-1-yl) ethyl)azanediyl))diacetic acid was presented as a redox-switchable ^{19}F MRI probe, highlighting the interest in this class of Fe(III) systems for biomedical applications. [24]

Building upon our previous work concerning Fe(III) complexes bearing tertiary amides (as illustrated in Scheme 1), we established that structural modifications led to systematic changes in the key molecular parameters governing relaxivity. [21] Specifically, we observed alterations in the inner-sphere water exchange rate as well as in the thermodynamic and kinetic stability of the complexes. In the present work, we extend this structural investigation to a second set of CDTA amide derivatives, focusing specifically on secondary amides. We selected the mono- and bis-butylamide derivatives of CDTA (namely, CD3A-BA and $CD2A-BA_2$, depicted in Scheme 1) to systematically explore the impact of increasing amide substitution on the resulting molecular and relaxation properties.

The main objective of this study is to investigate how the replacement of tertiary amide groups with secondary ones on the CDTA scaffold influences the structural, electronic, and relaxometric properties of the resulting Fe(III) complexes. Secondary amides differ from their tertiary counterparts in the basicity of the amide nitrogen, a factor that can significantly impact key molecular parameters as well as the thermodynamic and kinetic stability of the complex. In addition to detailed physicochemical characterization, we also evaluated the cellular toxicity of the synthesized Fe(III) chelates to provide an initial assessment of their safety profile and to gauge the potential of related Fe(III)-CDTA derivatives for future in vivo MRI applications.

2. Experimental section

2.1. Materials

All reagents were purchased from Merck (Darmstadt, Germany), Fluka (Buchs, Switzerland), and BLD Pharm (Shanghai, China), and used without further purification. The chemicals used for the experiments were of the highest analytical grade. $Fe(NO_3)_3$ was prepared by dissolving Fe_2O_3 (99.9%, Fluka) in 6 M HNO_3 and evaporating of the excess acid. The solid $Fe(NO_3)_3$ was dissolved in 0.1 M HNO_3 solution. The concentration of the $Fe(NO_3)_3$ solution was determined by using the standardized Na_2H_2EDTA in excess. The excess of the Na_2H_2EDTA was measured with standardized $ZnCl_2$ solution and xylenol orange as indicator. The H^+ concentration of the $Fe(NO_3)_3$ solution was determined by pH potentiometric titration in the presence of Na_2H_2EDTA excess. The concentration of the protonated CD3A-BA, $CD2A-BA_2$ ligands, and H_2HBED (HBED = *N*, *N*′-bis(2-hydroxybenzyl)ethylenediamine-N,N′-diacetic acid) solution was determined by pH-potentiometric titrations in the presence and absence of a 40-fold excess of Ca^{2+}. The pH-potentiometric titrations were made with standardized 0.2 M NaOH.

2.2. Synthesis of (4,4′-((1S,2S)-cyclohexane-1,2-diyl)bis(morpholine-2,6-dione)) (CDTAA)

0.5 g of CDTA (BLD Pharm, 1.44 mmol) were suspended in 2.6 mL of acetic anhydride (Merck, 20 equivalents) and 0.44 mL of pyridine (Merck, 4 equivalents). The mixture was stirred overnight at room temperature under nitrogen (N_2). To precipitate the anhydride, 100 mL of diethyl ether were slowly added to the reaction mixture, followed by centrifugation at room temperature (4000 rpm for 15 *min*) to separate the precipitate. This process was repeated three times. The resulting solid was then dried under vacuum overnight. [25] The yield was 83.4%, giving 372 mg of CDTAA. ^1H NMR (500 MHz, DMSO-d_6) δ (ppm): 3.81–3.67 (dd, $J = 17.4$ Hz, 8H, $CH_2 - CO$), 2.74 (d, 2H, ring CH), 1.69–1.58 (m, 4H, ring CH_2), 1.23–1.04 (m, 4H, ring CH_2). ^{13}C NMR (126 MHz, DMSO-d_6) δ (ppm): 166.55 (C=O), 61.63 (CH_2CO), 49.29 (ring CH), 27.59 (ring CH_2), 24.92 (ring CH_2).

2.3. Synthesis of 2,2′-(((1S,2S)-2-((carboxymethyl)(2-(diethylamino)-2-oxoethyl)amino)cyclohexyl)azanediyl)diacetic acid (CD3A-BA)

150 mg of CDTAA (0.48 mmol) were reacted with 48.5 μl of butylamine (Merck, 99.5%, 0.48 mmol) in 5 mL of anhydrous *N,N*-diethyldimethylacetamide (Merck, DMA). The solution was stirred overnight at 373 K under an inert atmosphere (N_2). Upon cooling to room temperature, the solution was washed four times with 50 mL of cold diethyl ether. The crude product was purified by preparative HPLC-MS using an Atlantis C18 column, with a linear gradient from 80:20H_2O/ACN to 100% ACN over 15 min at a flow rate of 5 mL/min. After solvent removal, 72.3 mg of the solid CD3A-BA were collected and vacuum-sealed (Yield = 45.2%). (ESI+): *m/z* calcd. *F*or $C_{18}H_{32}N_3O_7^+$: 402.47; found: 402.40 ($M + H^+$). ^{1}H NMR (500 MHz, MeOD, 320 K, Fig. S1A) δ (ppm): 1.01 (t, 3H); 1.36 (m, 3H); 1.44 (m, 4H); 1.59 (m, 2H); 1.91 (m, 3H), 2.25 (m, 2H), 2.71 (m, 1H), 3.04 (m, 1H); 3.34 (m, 8H). ^{13}C NMR (126 MHz, MeOD, 320 K, Fig. S1B) δ (ppm): 12.74 (-CH_3) 19.81 (-CH_2-) 23.35 (-CH_2-) 24.22 (-CH_2-) 24.27 (-CH_2-) 24.39 (-CH_2-) 24.50 (-CH_2-) 31.03 (-CH_2-) 31.72 (-CH-) 32.78 (-CH-) 38.82 (-CH_2-) 51.00 (-CH_2-) 60.31 (-CH_2-) 62.69 (-CH_2-) 162.15 (-CONH-) 170.71 (-COOH) 171.9 (-COOH, -COOH).

2.4. Synthesis of 2,2′-(((1S,2S)-cyclohexane-1,2-diyl)bis((2-(diethylamino)-2-oxoethyl)azanediyl))diacetic acid (CD2A-BA_2)

For the synthesis of the CD2A-BA_2 ligand, a similar procedure with respect to the mono-amide was followed. 150 mg of CDTAA (0.48 mmol) were added in butylamine (5 mL), which served both as the reagent and solvent. The solution was stirred overnight at 373 K under an inert nitrogen atmosphere (N_2). After cooling to room temperature, the solution was washed four times with 50 mL of cold diethyl ether. To remove any residual butylamine, the sample was passed through a column of Dowex C350Na ion-exchange resin. The product was then dried under vacuum, yielding 135.9 mg of white solid at the end of the reaction. (Yield = 60.4%). (ESI+): *m/z* calcd. *F*or $C_{22}H_{41}N_4O_6^+$: 457.59; found: 457.64 ($M + H^+$), 479.60 ($M + Na^+$). ^{1}H NMR (500 MHz, MeOD, 320 K, Fig. S2A) δ (ppm): 1.02 (t, 6H); 1.45 (m, 8H); 1.62 (m, 4H); 1.94 (m, 2H); 2.27 (m, 3H), 3.33 (m, 8H), 3.91 (m, 6H). ^{13}C NMR (126 MHz, MeOD, 320 K, Fig. S2B) δ (ppm): 12.65 (-CH_3,-CH_3) 19.68 (-CH_2-, -CH_2-, -CH_2-, -CH_2-) 23.89 (-CH_2-, -CH_2-) 30.81 (-CH_2-, − CH_2-) 39.03 (-CH-CH-) 52.3 (-CH_2-, -CH_2-) 62.5 (-CH_2-, -CH_2-); 161.6 (-CONH-); 167.7 (-COOH) 170.5 (-COOH, -COOH).

2.5. Synthesis of Fe(III) chelates

[Fe(CD3A-BA)] and [Fe(CD2A-BA_2)]$^+$ were synthetized following the same protocol. In detail, 20 mg of the ligand were dissolved in 5 mL of ultrapure water. The concentrations of the CD3A-BA and CD2A-BA_2 ligands were determined through pH-potentiometric titrations, conducted both in the presence and absence of a 40-fold excess of Ca^{2+}. After adjusting the pH to 2.5 using 0.5 M HCl, $Fe(NO_3)_3$ was then added in stoichiometric quantity. The concentration of the $Fe(NO_3)_3$ solution was established by titration with an excess of standardized Na_2H_2EDTA. The pH was corrected to 2.5 using 0.1 M NaOH. The solutions were stirred overnight. ESI-MS analysis of the Fe(III) chelates confirms the absence of free ligand, ensuring the purity of the obtained complexes: [Fe(CD3A-BA)] (ESI+): *m/z* calcd. *F*or $C_{18}H_{29}FeN_3O_7^+$: 455.29; found: 455.28 (M^+H^+). [Fe(CD2A-BA_2)]$^+$ (ESI+): m/z calcd. *F*or $C_{22}H_{38}FeN_4O_6^+$: 510.21; found: 510.56 (M^+).

2.6. Equilibrium measurements

2.6.1. pH-Potentiometry

The stability and protonation constants of Fe(III) complexes formed with CD3A-BA and CD2A-BA_2 ligands were determined by pH-potentiometric and spectrophotometric studies. The protonation and dimerization constants of the [Fe(CD3A-BA)] and [Fe(CD2A-BA_2)]$^+$ complexes were determined using pH-potentiometry by titrating the pre-prepared complexes from pH = 1.7 to pH = 12 with 0.2 M NaOH ([FeL] = 0.01 M). For the pH measurements and titrations, a *Metrohm 888 Titrando* titration workstation and a *Metrohm*-6.0234.110 combined electrode were used. Equilibrium measurements were carried out at a constant ionic strength (0.15 M $NaNO_3$) and at 298 K in 6 mL solutions of the samples. The solutions were stirred and N_2 was bubbled through them. The titrations were made in the pH range of 1.7–12.0. KH-phthalate (pH = 4.005) and borax (pH = 9.177) buffers were used to calibrate the pH meter, whereas for the calculation of [H^+] from the measured pH values we utilized the method proposed in the literature. [26] Specifically, a 0.01 M HNO_3 solution was titrated with standardized NaOH solution at 0.15 M $NaNO_3$ ionic strength. The differences (A) between the measured (pH_{read}) and calculated pH ($-\log[H^+]$) values were used to obtain the equilibrium H^+ concentration from the pH values measured in the titration experiments (A = 0.04). For equilibrium calculations, the stoichiometric ionic product of water (pK_w) must also be evaluated to calculate [OH^-] values under basic conditions. The V_{NaOH}-pH_{read} data pairs of the HNO_3 − NaOH titration obtained in the pH range 10.5–12.0 were used to calculate the pK_w value ($pK_w = 13.77$).

2.6.2. Capillary electrophoresis

The stability constants of [Fe(CD3A-BA)] and [Fe(CD2A-BA_2)]$^+$ were determined with Capillary Zone Electrophoresis (CZE) by following the competition reaction in the Fe^{3+}-CD3A-BA-CDTA and Fe^{3+}-CD2A-BA_2-EDTA systems at pH = 3.5. Two series of eight samples were prepared with [Fe^{3+}] = [CD3A-BA] = 1.00 mM and [CDTA] = 0.00, 0.25, 0.50, 1.00, 1.50, 2.00, 3.00 and 4.00 mM, [Fe^{3+}] = [CD2A-BA_2] = 1.00 mM and [EDTA] = 0.00, 0.25, 0.50, 1.00, 1.50, 2.00, 3.00 and 4.00 mM in 0.15 M $NaNO_3$ solution. The pH was adjusted to 3.2 by stepwise addition of concentrated NaOH and HNO_3 solutions. The samples were kept at 298 K for two weeks to ensure equilibrium is achieved (the time needed to reach the equilibria were determined by CZE). For the calculations of the stability constants of [Fe(CD3A-BA)] and [Fe(CD2A-BA_2)]$^+$, the molar integral values of [Fe(CD3A-BA)], [Fe(CD2A-BA_2)]$^+$, [Fe(CDTA)]$^-$ and [Fe(EDTA)]$^-$ were determined by recording the CZE electropherogram of 0.25, 0.50, 1.00 and 1.50 mM solutions of the Fe(III)-complexes. A *Hewlett-Packard HP3D* capillary electrophoresis system was used for CZE analyses. Separations were performed using bare fused-silica capillaries of 64 cm × 50 μm i.d. (*Agilent*). Before the first use, the capillary was washed with 1.0 M NaOH (15 min), 0.1 M NaOH (30 min) and the buffer electrolyte (30 min). Prior to CZE analysis, all buffers were filtered through a 0.45 μm syringe filter and stored in refrigerator at 277 K. In CZE the sample solutions were introduced at the anodic end of the capillary in normal mode (50 mbar, 2 s). The effective length of the capillary was 56 cm. The capillary was preconditioned with the buffer electrolyte (50 mM disodium hydrogen phosphate, pH = 6.0) for 3 *min*. The separation was performed at 298 K with the application of 25 kV voltage. After analysis, post conditioning (0.1 M NaOH) (3 min) and buffer washing (3 min) were run to remove all possible adsorbed materials from the capillary. In all measurements, 1 mM methyl orange as internal standard was applied to correct the migration time of the components on the electropherogram. The detection was carried out by on-column DAD measurement at 200 nm. The electropherograms were recorded and processed by the ChemStation B.04.02 version (Agilent). The individual linear regression equations (response-concentration) for all the Fe(III)-complexes were determined according to four concentrations. The peak areas were found to be linear ($R_2 \geq 0.998$) in a 0.25–1.50 mM concentration range of the complexes (precision better than 4%). The protonation and stability constants were calculated using the PSEQUAD program. [27]

2.7. Transchelation studies

2.7.1. Ligand-exchange kinetics with HBED

The kinetic inertness of the [Fe(CD3A-BA)] and $[Fe(CD2A\text{-}BA_2)]^+$ was evaluated by analyzing the rates of the transchelation reactions with the HBED ligand. The exchange reactions with HBED were studied by spectrophotometry, following the formation of the $[Fe(HBED)]^-$ complexes at 485 nm with *PerkinElmer Lambda 365* UV–Vis spectrophotometer. The concentration of the FeL complex was 0.2 mM, while the concentration of HBED was 10 and 20 times higher, in order to guarantee pseudo-first-order conditions. The temperature was maintained at 298 K and the ionic strength of the solutions was kept constant, 0.15 M for $NaNO_3$. The exchange rates were studied in the 9.5–12.5 pH range. Piperazine (pH range 8.5–10.5) and Na_2HPO_4 (pH range 11.0–12.5) buffers (0.01 M) were used in order to stabilize the pH. The pseudo-first-order rate constants (k_d) were calculated by fitting the absorbance data with Eq. 1.

$$A_t = (A_0 - A_p)e^{-k_d t} + A_p \quad (1)$$

where A_t, A_0, and A_p are the absorbance values at time t, at the start of the reaction, and at equilibrium, respectively. Calculations of the kinetic parameters were performed by the fitting of the absorbance – time data pairs with Eq. (1), with the Micromath Scientist computer program (version 2.0, Salt Lake City, UT, USA).

2.7.2. Ligand-exchange kinetics with transferrin

The ligand exchange reaction of $[Fe(CD2A\text{-}BA_2)]^+$ and [Fe(CD3A-BA)] with human serum transferrin (sTf, Sigma, partially Fe^{3+} saturated) have been studied by spectrophotometry, following the formation of Fe(III)-transferrin complexes (Fe(sTf) and Fe_2(sTf)) using Cary 3500 spectrophotometer and 1 cm cells at 460 nm. The concentration of Fe (III) complexes was 0.25 mM, while that of the sTf was 50 μM in order to ensure pseudo-first-order conditions. The exchange rates were studied at pH = 7.4. For keeping the pH values constant, 0.01 M HEPES was used. The concentration of the human serum transferrin solution was determined from the absorbance at 280 nm using the molar absorptivity ε_{280} = 91,200 cm^{-1} M^{-1}. [28] The temperature was maintained at 25 °*C*, the ionic strength and the sodium hydrogen-carbonate concentration of the samples was kept constant; 0.15 M for NaCl and 0.025 M for $NaHCO_3$, respectively. Rates of ligand-exchange reaction can be expressed by Eq. 2:

$$-\frac{[FeL]_t}{dt} = \frac{d[Fe_x(sTf)]}{dt} = k_d[FeL]_t \quad (2)$$

where k_d is a pseudo-first-order rate constant, $[FeL]_t$ and $[Fe_x(sTf)]$ are the concentration of $Fe(CD2A\text{-}BA_2)]^+$, [Fe(CD3A-BA)] and [Fe(sTf)] complexes at the time t, respectively (x = 1 or 2). During the progress of the ligand-exchange reactions the concentration of the $[Fe_x(sTf)]$ species increases, while that of the [FeL] decreases. By the use of 1.0 cm cells, the first-order rate constant, k_d can be expressed by Eq. (1) as:

$$k_d = \frac{\Delta Abs}{dt} \times \frac{1}{\varepsilon_{Fe_x(sTf)}} \times \frac{1}{[FeL]_t} \quad (3)$$

In the Eq. (3) ΔAbs is the increase of the absorbance value during the time Δ*t* and $\varepsilon_{Fex(sTf)}$ is the molar absorptivity of the $[Fe_x(sTf)]$ complex at 460 nm ($\varepsilon_{Fex(sTf)}$ = 2204 M^{-1} cm^{-1}). The absorption of the $[Fe(CD2A\text{-}BA_2)]^+$ and [Fe(CD3A-BA)] complexes can be neglected at 460 nm. In the calculations, a 10% conversion of sTf was derived from the initial slopes of the kinetic traces (ΔAbs/dt) for both the [Fe(CD3A-BA)]-sTf and $[Fe(CD2A\text{-}BA_2)]^+$-sTf systems. The saturation of the human serum transferrin with Fe^{3+} was determined by spectrophotometric titration of the transferrin with standardized $Ga(NO_3)_3$ solution at pH = 7.4 and 25 °*C* in 0.025 M $NaHCO_3$ and 0.15 M NaCl solution in the wavelength range 240–250 nm.

2.8. Cyclic voltammetry

Cyclic voltammetry measurements were carried out by using an *Autolab PGSTAT12 electrochemical analyzer* (Eco Chemie, Utrecht, The Netherlands) connected to a personal computer running GPES 4.9 electrochemical software. A standard three-electrode cell was constructed so that the tip of the reference electrode (Ag/AgCl, 3 M KCl) was close to the working electrode (a disk of glassy carbon (GC), diameter 0.1 cm, sealed in epoxy resin). The GC working electrode was polished with alumina, rinsed with distilled water, and dried. This procedure resulted in an almost completely reproducible surface for all experiments. Measurements were performed under nitrogen in milliQ water containing 0.1 M KNO_3 as supporting electrolyte; the pH was set with nitric acid. The Fe(III) complex concentration was 1 mM. The temperature of the solution was kept constant (298 ± 1 K) by the circulation of a water/ethanol mixture through a jacketed cell. Positive feedback iR compensation was applied routinely. All peak potentials were measured at a scan rate of 0.2 V s^{-1} and reported vs. the reference electrode.

2.9. Relaxometric analysis

^{1}H NMRD profiles were acquired utilizing a fast-field cycling Stelar SmartTracer relaxometer (Mede, Pavia, Italy), with magnetic-field strength varying from 0.00024 *to* 0.25 T (0.01–10 MHz range). The $1/T_1$ values were measured with an absolute uncertainty of ±1%. Temperature control was achieved using a Stelar VTC-91 airflow heater equipped with a calibrated copper-constantan thermocouple (uncertainty of ±0.1 K). Data at higher fields (0.5–3 T, corresponding to 20–120 MHz proton Larmor frequency) were gathered with a High Field Relaxometer (Stelar) outfitted with the HTS-110 3 T Metrology Cryogen-free Superconducting Magnet. The measurements were conducted employing a standard inversion recovery sequence (20 experiments, 3 scans) with a typical 90° pulse width of 3.5 μs, and data reproducibility fell within ±0.5%. Variable pH relaxivity measurements of [Fe(CD3A-BA)] and $[Fe(CD2A\text{-}BA_2)]^+$ were carried out by direct titration of the samples in the pH range 3.0–11.0 (1.5 T, 0.15 M $NaNO_3$ and 298 K). The pH was adjusted by stepwise addition of concentrated NaOH or HNO_3 solution. Stability tests in Seronorm® were performed by adding 90.0 mg of the corresponding lyophilized solid to 1.0 mL of a 1.0 mM solution of the complex under study.

2.10. NMR measurements

^{1}H and ^{13}C NMR spectra were recorded at 298 K using a Bruker Avance III spectrometer (11.7 T) spectrometer equipped with a 5 mm probe and a Bruker BVT 3200 control unit. Variable ^{17}O NMR measurements were recorded on aqueous solution of the complexes (≈ 4 mM) enriched to reach 2.0% of the ^{17}O isotope (Cambridge Isotope). Transverse relaxation rates were determined by measuring the signal width at half-height as a function of temperature within the range of 278–350 K. The effective magnetic moments of the Fe(III) complexes were measured by using Evans′ method on the same spectrometer, by knowing the exact concentration of Fe(III) in solution (ICP-MS). The effective magnetic moments for [Fe(CD3A-BA)] and $[Fe(CD2A\text{-}BA_2)]^+$ were found to be 5.9 B.M at pH 6.5. The simultaneous fitting of ^{1}H NMRD profiles and ^{17}O NMR data was conducted using the Micromath Scientist computer program (version 2.0, Salt Lake City, UT, USA).

2.11. In vitro cytotoxicity assay

The cytotoxicity of the Fe(III) complexes was assessed using the Sulforhodamine B (SRB) Cytotoxicity Assay Kit (Canvax Biotech), following the manufacturer's instructions. Cells (4000 per well) were seeded in 96-well plates and exposed to increasing concentrations of the Fe(III) complexes for the indicated incubation time. After treatment, cells were fixed, stained with SRB, and the bound dye was solubilized for

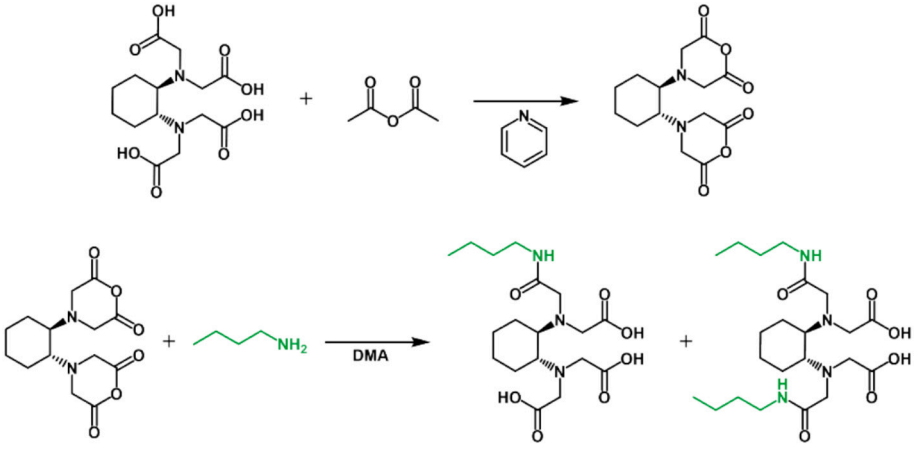

Scheme 2. Synthesis of amide-derivatives of CDTA ligands.

absorbance measurement at 565 nm using a microplate reader (Thermo Scientific™ Varioskan™ LUX Multimode Microplate Reader). Reference compounds were tested in three independent biological replicates (each with three technical replicates), whereas Fe(III) complexes were analyzed in five biological replicates. Cell viability was calculated as the percentage of absorbance relative to untreated controls, and the resulting dose-response curves were used to estimate IC_{50} values.

3. Results and discussion

3.1. Synthesis

The CD3A-BA and CD2A-BA_2 ligands were synthesized following a previously established procedure, which was recently adapted for preparing related Fe(III) chelators (Scheme 2). [25] The starting material, H_4CDTA, was first converted into its dianhydride intermediate by reaction with acetic anhydride in the presence of pyridine. The resulting dianhydride was then reacted with butylamine. Critically, the stoichiometric ratio between the anhydride intermediate and the butylamine was precisely controlled to selectively optimize the yield of either the mono- or bis-amide CDTA derivative. In particular, a 1:1 *M* ratio (anhydride: butylamine) was employed to selectively favor the formation of the monoamide derivative (CD3A-BA). Conversely, using an excess of butylamine facilitated the complete substitution, thus favoring the isolation of the bisamide derivative (CD2A-BA_2). The products were characterized using ^{1}H and ^{13}C NMR spectroscopy and ESI^+ mass spectrometry, with reaction yields between 45 and 60%. (detailed information in the experimental section).

The corresponding Fe(III) complexes were subsequently obtained using the same synthetic procedure. Briefly, 20 mg of the synthesized ligand was reacted with an equimolar amount of $Fe(NO_3)_3$ in an aqueous solution initially maintained at pH 2.5. The reaction mixture was stirred overnight to ensure complete complexation, after which the pH was carefully adjusted to 7.2. The successful formation of the complexes was confirmed by ESI^+ mass spectrometry (more details in the experimental section).

3.2. Thermodynamic studies

The thermodynamic properties of the CD3A-BA and CD2A-BA_2 ligands, together with their corresponding Fe(III) complexes, were investigated through the determination of their protonation and stability constants using pH-potentiometry, UV–visible spectrophotometry, Capillary Zone Electrophoresis (CZE), Cyclic Voltammetry (CV) and ^{1}H NMR relaxometry. Detailed experimental procedures and the equations employed for the equilibrium calculations are provided in the Electronic Supporting Information (ESI, Eqs. S1-S7, Figs. S3 - S8). The obtained results, summarized in Table 1, are compared with those previously reported for CD3A-DEA, CD2A-DEA_2, and the parent ligands CDTA and EDTA. The basicity of the nitrogen atoms in EDTA-like ligands can be influenced by four main factors: i) electrostatic repulsion between protonated nitrogen atoms, which decreases the basicity of the remaining macrocyclic nitrogens; ii) hydrogen bonding between a protonated nitrogen atom and a negatively charged carboxylate group, which tends to increase the nitrogen basicity; iii) the formation of relatively stable Na(I) complex (e.g., $[Na(CDTA)]^{3-}$; $\log K_{NaL} = 4.66$) [29], which results in a reduction of the ligand's overall basicity; and iv) electron-donating or -withdrawing effects of substituents on the ligand backbone and pendant arms. As shown in Table 1, replacing negatively charged carboxylate groups with neutral amide functionalities significantly affects the acid–base behavior of the ligands in solution, consistent with previous observations for the corresponding diethyl- and piperidine-amide derivatives. [21,24,30] The protonation constants ($\log K_1^H$ and $\log K_2^H$, associated with the protonation of the nitrogen donor atoms) of CD2A-

Table 1
Protonation constants of CD3A-BA, CD2A-BA_2, CD3A-DEA, CD2A-DEA_2, CDTA and EDTA (25 °*C*).

	CD3A-BA	CD2A-BA_2	CD3A-DEA[a]	CD2A-DEA_2[a]	CD2A2Am-CF_3Pip[b]	CDTA[c]	EDTA[c]
I	0.15 M $NaNO_3$						
$\log K_1^H$	10.31 (2)	8.69 (4)	9.11	8.54	8.62	9.54	9.40
$\log K_2^H$	4.64 (4)	4.25 (6)	5.21	5.07	4.95	6.08	6.10
$\log K_3^H$	2.79 (4)	1.65 (5)	3.34	2.57	2.13	3.65	2.72
$\log K_4^H$	1.51 (7)	–	2.32	–	–	2.69	2.08
$\log K_5^H$	1.4 (1)	–	0.6	–	–	1.14	1.23
$\Sigma\log K_i^H$	20.65	14.59	20.58	16.18	15.70	23.10	21.53

[a] Ref [21].
[b] Ref [24].
[c] Ref [23].

Table 2
Stability, protonation and conditional stability constants (pFe) and the formal electrode potentials values ($E^{\circ\prime}$) values of the Fe(III)-complexes of CD3A-BA, CD2A-BA_2, CD3A-DEA, CD2A-DEA_2 and CDTA (25 °*C*).

	[Fe(CD3A-BA)]	[Fe(CD2A-BA_2)]$^+$	[Fe(CD3A-DEA)][a]	[Fe(C2A-DEA_2)]$^+$ [a]	[Fe(CD2A2Am-CF_3Pip)]$^+$ [b]	[Fe(CDTA)]$^-$ [c]	[Fe(EDTA)]$^-$ [c]
I	0.15 M $NaNO_3$						
$\log K_{ML}$	21.8 (3)	19.2 (1)	22.5	20.9	21.42	24.36	22.14
$\log K_{MHL}$	1.36 (5)	–	1.63	–	–	1.77	1.12
$\log K_{MLH_{-1}}$	8.54 (9)	7.19 (9)	9.03	8.74	8.13	9.50	7.51
$\log K_{MLH_{-2}}$	–	9.2 (1)	–	–	–	–	–
$\log K_D$	14.42 (9)	12.78 (9)	17.38	15.06	15.13	17.64	13.00
$\log K_d$	2.66 (9)	1.61 (9)	0.69	2.43	1.43	1.40	2.02
pFe[d]	18.39	17.51	20.28	19.27	–	21.67	19.47
$E^{\circ\prime}$ (V vs. NHE)	+0.181	+0.261	–	–	+0.240	+0.102	+0.110

[a] Ref [21].
[b] Ref [24].
[c] Ref [23].
[d] pFe = $-\log[Fe^{3+}]_{free}$, $[Fe^{3+}]_{tot} = 1 \times 10^{-6}$ M, $[L]_{tot} = 10 \times 10^{-6}$ M, pH = 6.0.

BA_2 decrease by 0.85 and 1.44 log K units, respectively, relative to the parent CDTA.

This reduction, well-documented in polyaminocarboxylate derivatives, arises from the electron-withdrawing effect of the amide groups, which decreases the basicity of the amine nitrogens. In contrast, CD3A-BA exhibits a higher first protonation constant than CDTA (10.31 vs. 9.54). Since the amide group in the CD3A-BA ligand also possesses electron-withdrawing properties and forms weaker hydrogen bonds with the protonated nitrogen atoms, the higher protonation constant of CD3A-BA is most likely due to the formation of a less stable Na(I) complex compared to CDTA. The second protonation constant, however, follows a similar decreasing trend to that observed for the CDTA diethylamide analogues. Overall, these results align with the established protonation behavior reported for CDTA and DTPA and their corresponding amide derivatives. [30,31] As expected, the reduced protonation constants of the ligands directly influence both the stability and protonation constants of the Fe(III) complexes (Table 2).

Substitution of one or two carboxylate groups in CDTA with secondary amide functionalities leads to a marked decrease in the stability constants of the corresponding Fe(III) complexes - by 2.56 and 4.86 log*K* units for [Fe(CD3A-BA)] and [Fe(CD2A-BA2)]$^+$, respectively, relative to [Fe(CDTA)]$^-$. This reduction reflects the weaker coordination ability of neutral amide oxygen atoms compared to negatively charged carboxylate oxygens. A similar trend has been reported for Gd(III) complexes, where DTPA derivatives containing mono- and bis-amide substituents (DTPA-N′-MA, DTPA-N-MA, and DTPA-BMA) exhibit lower stability than the parent DTPA ligand. [31,32] Interestingly, the tertiary diethyl- and piperidine-amide derivatives consistently form more stable Fe(III) complexes than the corresponding secondary butylamide analogues ($\Delta\log K \approx -0.7$ for CD3A-BA and − 2.2 for CD2A-BA_2). This difference can be rationalized by considering the distinct electronic environments of the amide carbonyl oxygens. In tertiary amides, the stronger inductive effect and increased steric rigidity imparted by the ethyl or piperidine substituents enhance the electron density on the carbonyl oxygen, increasing its basicity and thus its affinity for Fe(III). Consequently, the tertiary amide derivatives yield higher overall stability constants for their Fe(III) chelates.

Weaker coordination of the amide group in a respect to the negatively charged acetic acid pendant arms to Fe(III) ion is also supported by the lower conditional stability (pFe) of the [Fe(CD3A-BA)], [Fe(CD2A-BA_2)]$^+$, [Fe(CD3A-DEA)] and [Fe(CD2A-DEA_2)]$^+$ than that of [Fe(CDTA)]$^-$. Cyclic Voltammetry measurements reveal that both [Fe(CD3A-BA)] and [Fe(CD2A-BA_2)]$^+$ are reduced at more positive potentials than [Fe(CDTA)]$^-$ due to the lower selectivity for Fe(III) over Fe(II) by CD3A-BA and CD2A-BA_2 than by CDTA. The $E^{\circ\prime}$ of [Fe(CD3A-BA)] is slightly more positive than that of [Fe(CD2A-BA_2)]$^+$. On the other hand, ΔE_p values of [Fe(CD3A-BA)], [Fe(CD2A-BA_2)]$^+$ and [Fe(CDTA)]$^-$ (>59 mV, Table S1) indicate an electrochemically quasi-reversible (slow) electron transfer related to a difficult rearrangement of the ligand around the metal ion in the +2 oxidation state after the reduction step.

As a consequence of the higher residual positive charge of [Fe(CD3A-BA)] and [Fe(CD2A-BA_2)]$^+$ compared to [Fe(CDTA)]$^-$, the equilibrium constants for deprotonation of the coordinated water molecule (log $K_{FeLH_{-1}}$) are lower by 0.96 and 2.31 log*K* units, respectively, relative to the corresponding mono- and bis-diethylamide analogues. [21] The increased residual charge, together with the reduced deprotonation constant of the inner-sphere water molecule, also enhances the tendency of these complexes to form oxo-bridged dimers, which exhibit characteristic antiferromagnetic coupling between the two Fe(III) centers. This behavior is indeed observed for both [Fe(CD3A-BA)], [Fe(CD2A-BA_2)]$^+$ and [Fe(CD2A2Am-CF_3Pip)]$^+$ as indicated by the K_D and K_d values

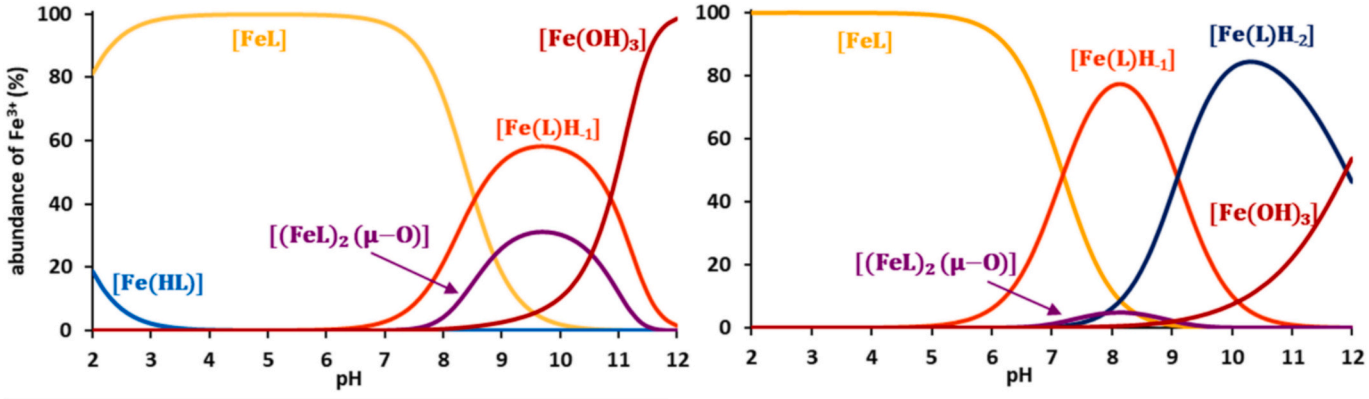

Fig. 1. Species distribution of [Fe(CD3A-BA)] (left) and [Fe(CD2A-BA_2)]$^+$ (right) ([Fe^{3+}] = [L] = 1.0 mM, 25 °*C* in 0.15 M $NaNO_3$).

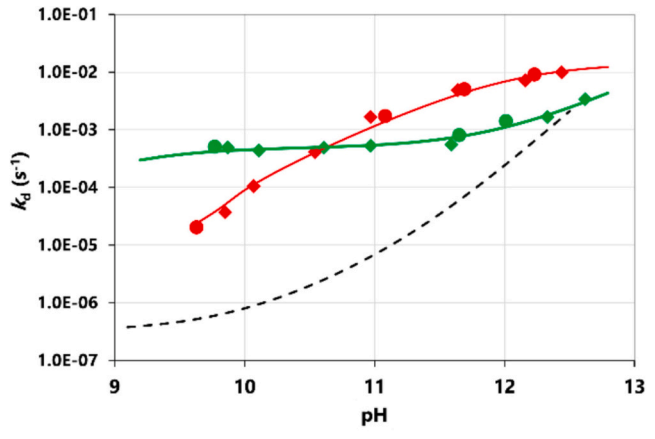

Fig. 2. Pseudo-first order dissociation rate constant as a function of pH. ([FeL] = 0.2 mM, [HBED] = 2 mM (◆); [HBED] = 4 mM (•); lines are fitted values. 0.15 M $NaNO_3$, *25 °C*). [Fe(CD3A-BA)] (red) and $[Fe(CD2A\text{-}BA_2)]^+$ (green) and dashed lines are for $[Fe(CDTA)]^-$. [23]. *(For interpretation of the references to colour in this figure legend, the reader is referred to the web version of this article.)*

reported in Table 2. These findings confirm that replacing one or more carboxylate groups with secondary amide functions increases the acidity of the coordinated water molecule, thereby promoting dimerization through oxo-bridge formation. Furthermore, a second deprotonation process is detected for $[Fe(CD2A\text{-}BA_2)]^+$, which may arise from deprotonation of the amide -NH group. This is likely facilitated by the overall positive charge of the complex and the strong polarizing effect of the Fe (III) center. Based on the equilibrium constants listed in Table 2, the species distribution diagrams for the [Fe(CD3A-BA)] and $[Fe(CD2A\text{-}BA_2)]^+$ systems were computed as a function of pH (Fig. 1).

The speciation diagrams of the two complexes reveal distinct behaviors. While both systems predominantly exist as the mononuclear Fe (III) species between pH 2.0 and 6.0, notable differences emerge at higher pH values. The formation of oxo-bridged dimers is considerably more pronounced for the monoamide complex than for the bisamide analogue. This discrepancy likely arises from the second deprotonation process observed for $[Fe(CD2A\text{-}BA_2)]^+$, which decreases the overall positive charge of the complex, stabilizing the monomeric species and thus reducing its tendency to form oxo-bridged dimers. For both systems, although to different extents, the weaker interaction between Fe (III) and the neutral amide donors promotes the formation of $Fe(OH)_3$ species at pH values above 9.0. To confirm the dimer formation inferred from speciation analysis, relaxivity measurements were carried out as a function of complex concentration at the pH corresponding to dimer formation. [33] As shown in Fig. S7 (ESI), relaxivity decreases with increasing [FeL], consistent with the formation of Fe(III) oxo-bridged dimers. These dimeric species exhibit antiferromagnetic coupling between the two Fe(III) centers, leading to inefficient paramagnetic relaxation. Given that the formation of the oxo-bridged dimer is directly proportional to the concentration [FeL] of the complex (as defined in Eqs. S6 and S7, ESI), the observed trend provides strong experimental support for the proposed equilibrium.

3.3. Dissociation Kinetics

The kinetic inertness of the Fe(III) complexes was rigorously investigated through competitive transchelation reactions. Stability was assessed using two distinct, high-affinity challenges: the small-molecule chelator *N*,*N*′-bis(2-hydroxybenzyl)ethylenediamine-N,N′-diacetic acid (HBED), and the physiological iron transport protein, human serum transferrin (sTf). The detailed protocols for these competitive assays are described in the Materials and Methods section. HBED was chosen as the

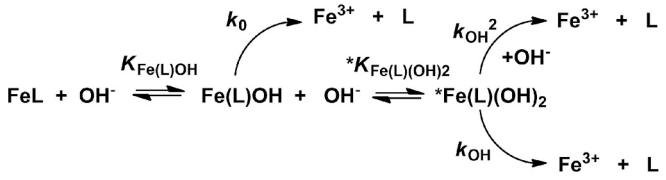

Scheme 3. The proposed reaction mechanism and rate law.

competing ligand owing to the very high thermodynamic stability of the $[Fe(HBED)]^-$ complex (log $K_{Fe(HBED)}$ = 39.68; 0.1 M KNO_3, *25 °C*), [34] which allows accurate monitoring of the transchelation process. Reactions were carried out using a large excess of HBED to ensure pseudo–first-order kinetic conditions. The resulting pseudo–first-order rate constants (k_d) for transchelation at different pH values are reported in Fig. 2.

The proposed mechanism for Fe(III) complex transchelation is illustrated in Scheme 3, while detailed definitions and the equations used for kinetic data analysis are provided in the ESI (Eqs. S8-S15, Figs. S9 and S10). The pH dependence of k_d indicates that complex dissociation proceeds via both spontaneous (k_0) and hydroxide-assisted pathways (k_{OH^1} and k_{OH^2}) of the $Fe(L)H_{-1}$ species within the investigated pH range.

The corresponding reaction mechanism and rate law are summarized in Electronic Supporting Information (ESI, Eqs. S8-S15). The fitted kinetic parameters are listed in Table 3. The dissociation of [Fe(CD3A-BA)] is predominantly governed by an OH^--assisted (k_{OH^2}) pathway, as evidenced by the dependence of k_d values on pH (Fig. 2). For the transchelation of $[Fe(CD2A\text{-}BA_2)]^+$ with HBED, the rate-determining step similarly involves OH^--assisted dissociation of the $Fe(L)H_{-1}$ species, followed by rapid capture of the released Fe(III) ion by HBED, consistent with the mechanism previously observed for the corresponding Fe(III) complexes with CD3A-DEA, $CD2A\text{-}DEA_2$ and CD2A2Am-CF_3Pip ligands. A comparison of the $t_{1/2}$ values at pH 10.0 for the Fe(III) complexes of CDTA and its BA, DEA and Am-CF_3Pip derivatives reveals the following stability trend: CDTA > CD3A-DEA > $CD2A\text{-}DEA_2$ ~ CD2A2Am-CF_3Pip > CD3A-BA > $CD2A\text{-}BA_2$. This progressive increase in dissociation rate can be rationalized in terms of donor group substitution. Replacing negatively charged carboxylate groups with neutral amide functions weakens Fe(III)–oxygen interactions, as amide oxygens possess lower electron density. Among amide derivatives, tertiary amides provide slightly higher electron density on the carbonyl oxygen than secondary ones, leading to stronger coordination and greater complex stability. The overall weakening of Fe (III)-ligand bonding facilitates faster intramolecular rearrangements of the CDTA framework and, consequently, more rapid Fe(III) release. In the BA derivatives, the $t_{1/2}$ values decrease by approximately two- to threefold, underscoring the pronounced destabilizing influence of secondary amide substitution - fully consistent with the observed thermodynamic data.

To further assess the kinetic inertness of the Fe(III) complexes under physiologically relevant conditions, transchelation reactions with human serum transferrin (sTf) were investigated. Transferrins are Fe^{3+}-transporting glycoproteins (≈80 kDa) that include serum transferrin (sTf), ovotransferrin (OTf), and lactoferrin (LTf), classified according to their biological origin and function. [35] In human serum, sTf is only ≈ 30% saturated with Fe^{3+}, providing a substantial reserve capacity to sequester iron released from labile complexes. Owing to its exceptionally high affinity for Fe^{3+}, transferrin can effectively compete with synthetic ligands for the metal ion, potentially facilitating the dissociation of Fe(III) complexes in vivo. [36] Since metal uptake by sTf requires the presence of a synergistic bicarbonate anion, experiments were performed at pH 7.4 and *25 °C* in 25 mM $NaHCO_3$ buffer. Spectrophotometric titration confirmed an Fe^{3+}-binding saturation of 28.7 ± 0.5%, in excellent agreement with the physiological value of approximately 30%.

Table 3
Rate (k_i), equilibrium constants (k_{OH^2}) and half-lives ($t_{1/2} = \ln 2/k_d$) characterizing the dissociation reactions of [Fe(CD3A-BA)] and $[Fe(CD2A\text{-}BA_2)]^+$ compared to related complexes (0.15 M $NaNO_3$, 298 K).

	[Fe(CD3A-BA)]	$[Fe(CD2A\text{-}BA_2)]^+$	[Fe(CD3A-DEA)] [a]	$[Fe(C2A\text{-}DEA_2)]^+$ [a]	$[Fe(CD2A2Am\text{-}CF_3Pip)]^+$ [b]	$[Fe(CDTA)]^-$ [c]	$[Fe(EDTA)]^-$ [c]
$k_0(s^{-1})$	–	–	–	4×10^{-6}	2×10^{-6}	3.2×10^{-7}	5×10^{-6}
k_{OH} (M^{-1} s^{-1})	0.8 ± 0.1	30 ± 2	2.4×10^{-2}	5×10^{-2}	0.77 / 0.09	3.4×10^{-3}	1.0
k_{OH^2} (M^{-1} s^{-1})	–	$(2.4 \pm 0.3) \times 10^3$	6	1.6×10^2	144 / 14	1.2	1.4
$^*K_{OH^2}$ (M^{-1})	60 ± 10 $logK_H = 12.04$	6.2×10^4 $logK_H = 9.2$	–	6×10^2 $logK_H = 11.02$	–	–	–
$k_d(s^{-1})$ at pH 10.0	1.30×10^{-4}	4.49×10^{-4}	4.08×10^{-6}	1.35×10^{-5}	1.24×10^{-4} / 1.56×10^{-5}	6.08×10^{-7}	1.65×10^{-4}
$t_{1/2}$(h) at pH 10.0	1.48	0.43	47.2	13.3	1.6 / 12.3	316.7	1.2

[a] Ref [21].
[b] Ref [24].
[c] Ref [23].

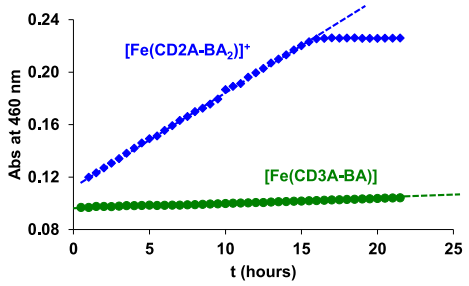

Fig. 3. Absorbance of the $[Fe(CD2A\text{-}BA_2)]^+$-sTf (green) and [Fe(CD3A-BA)]-sTf (blue) systems as a function of time at 460 nm ([FeL] = 2.5×10^{-4} M, [sTf] = 5.0×10^{-5} M, pH = 7.4, 0.025 M $NaHCO_3$, 0.01 M HEPES, 0.15 M NaCl, 25 °C). *(For interpretation of the references to colour in this figure legend, the reader is referred to the web version of this article.)*

Ligand-exchange reactions between [Fe(CD3A-BA)] and $[Fe(CD2A\text{-}BA_2)]^+$ and sTf (Eq. 4) were monitored spectrophotometrically at 460 nm, corresponding to the characteristic absorption band of the $[Fe_x(sTf)]$ adducts (x = 1, 2). The reactions were conducted under pseudo-first-order conditions, employing an excess of the Fe(III) complex.

$$FeL + sTf \; Fe_x(sTf) + L \quad (4)$$

In the presence of an excess of $[Fe(CD2A\text{-}BA_2)]^+$ and [Fe(CD3A-BA)], the ligand-exchange reaction can be treated as a pseudo-first-order process. Under these conditions, the reaction rate can be described by Eq. 2, where k_d represents the pseudo-first-order rate constant and $[FeL]_t$ is the total concentration of the Fe(III) complex. The rate of reaction ($-d[FeL]_t/dt$) and the corresponding k_d values were obtained from the slopes of the kinetic traces (ΔAbs/dt). Considering the molar absorptivity of the $[Fe_x(sTf)]$ species determined from the saturation titration of sTf with Fe^{3+} ($\varepsilon_{Fe(sTf)} = 2204$ M^{-1} cm^{-1}), the -d$[FeL]_t$/dt values were calculated from the kinetic curves (ΔAbs/dt, Fig. 3) according to Eq. 3.

The k_d values were calculated from the -d$[FeL]_t$/dt values using Eq. 3, assuming a total Fe(III) complex concentration of $[Fe(CD2A\text{-}BA_2)]^+$ = [Fe(CD3A-BA)] = 2.5×10^{-4} M. The obtained k_d and the half-life ($t_{1/2} = \ln 2/k_d$) values were 3.6×10^{-6} s^{-1} and 2.2 days for $[Fe(CD2A\text{-}BA_2)]^+$, and 1.6×10^{-7} s^{-1} and 51.3 days for [Fe(CD3A-BA)], respectively. These results are in good agreement with those derived from the HBED transchelation experiments. At pH 7.4 ($[OH^-] = 3.8 \times 10^{-7}$ M), the OH^--assisted dissociation rate constants ($k_1[OH^-]$) were calculated to be 3.0×10^{-7} s^{-1} for [Fe(CD3A-BA)] and 1.1×10^{-5} s^{-1} for $[Fe(CD2A\text{-}BA_2)]^+$, values comparable to those obtained for the sTf-mediated transchelation. These findings indicate that Fe(III) release in the presence of sTf likely proceeds via the same OH^--assisted dissociation pathway identified in the HBED studies. The significantly faster reaction observed for $[Fe(CD2A\text{-}BA_2)]^+$ can thus be attributed to its approximately 37-fold higher OH^--catalyzed dissociation rate (Table 3).

3.4. Relaxometric characterization

The proton relaxivity of the Fe(III) complexes was measured as a function of pH, temperature, and magnetic field strength. As for the parent $[Fe(CDTA)]^-$ complex, the investigated Fe(III) species are expected to adopt a heptacoordinated geometry, featuring one inner-sphere water molecule. However, due to the pronounced acidity of Fe(III), deprotonation of the coordinated water molecule is likely to occur - a phenomenon well documented for analogous complexes such as $[Fe(EDTA)]^-$ and supported by the potentiometric results. [23] Deprotonation of inner-sphere water exerts a marked influence on relaxivity through two main effects: (i) loss of a bound proton reduces the overall relaxivity contribution, and (ii) coordination of an OH^- ligand strengthens Fe—O interactions, substantially increasing the water

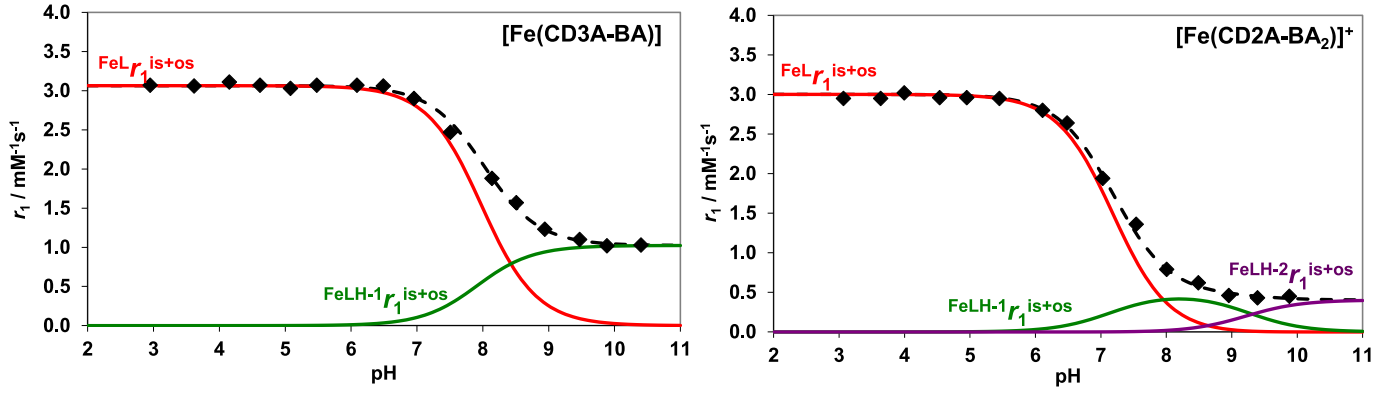

Fig. 4. Species distribution and relaxivity values as function of pH (◆) and fitted contributions of the different species for [Fe(CD3A-BA)] and $[Fe(CD2A\text{-}BA_2)]^+$ ([FeL] = 1 mM, 61 MHz, 298 K, 0.15 M $NaNO_3$).

Table 4
Relaxation and kinetic parameters characterizing the [Fe(CD3A-BA)] and [Fe(CD2A-BA_2)]$^+$ complexes (298 K and 61 MHz).

	[Fe(CD3A-BA)]	[Fe(CD2A-BA_2)]$^+$
$^{FeL}r_1^{is+os}$ (mM^{-1} s^{-1})	3.05 ± 0.02	3.00 ± 0.04
$^{Fe(L)H-1}r_1^{is+os}$ (mM^{-1} s^{-1})	1.22 ± 0.01	0.52 ± 0.02
$^{Fe(L)H-2}r_1^{is+os}$ (mM^{-1} s^{-1})	–	0.40 ± 0.02
T_{1pr} (μs)	–	13.7 ± 0.4
k_B (M^{-1} s^{-1})	–	(9 ± 2) × 10^5 (HEPES) (1.0 ± 0.4) × 10^{10} (piperazine)
k_{HB} (M^{-1} s^{-1})	–	(8 ± 4) × 10^5 (piperazine)

residence lifetime (τ_M) and consequently diminishing relaxivity. To determine the pH range in which the complexes retain a monohydrated form, relaxivity measurements were performed across the pH range 3.0–10.5 at 1.5 T and 298 K (Fig. 4).

The assumed monohydrated nature of the Fe(III) complexes is supported by the r_1 values obtained from the relaxivity profiles below pH 6.0: 3.1 mM^{-1} s^{-1} for [Fe(CD3A-BA)] and 3.0 mM^{-1} s^{-1} for [Fe(CD3A-BA_2)]$^+$, values consistent with those typically observed for monohydrated Fe(III) complexes. [13,21,37] As expected, the presence of amide substituents significantly affects the acidity of the coordinated water molecule, as evidenced by the marked decrease in r_1 with increasing pH when compared to the parent [Fe(CDTA)]$^-$ complex. [30,32] At basic pH, the observed reduction in r_1 for both complexes cannot be attributed solely to the deprotonation of the inner-sphere water molecule. The formation of μ-oxo-bridged dimeric species also contributes to the observed behavior, leading to antiferromagnetic coupling between the two Fe(III) centers, as discussed in the previous section. The pH dependence of the relaxivity was modeled by accounting for the inner- and outer-sphere contributions of each individual species present in solution.

The kinetic parameters and relaxivity values (representing the combined inner- and outer-sphere contributions) for the FeL, Fe(L)H$_{-1}$ and Fe(L)H$_{-2}$ species of the [Fe(CD3A-BA)] and [Fe(CD2A-BA2)]$^+$ complexes, obtained by the data fitting, are detailed in Table 4. The corresponding mathematical models and expressions are provided in the ESI.

Interestingly, pH-potentiometric data indicate a second deprotonation process for the [Fe(CD2A-BA_2)]$^+$ complex, which can likely be attributed to the deprotonation of an amide -NH group. This behavior arises from the positive charge of the complex and the strong polarization exerted by the Fe(III) center. The resulting labile amide protons are capable of participating in prototropic exchange processes, mechanisms that can enhance the efficiency of paramagnetic probes by facilitating proton relaxation of bulk water molecules. However, the prototropic exchange process is relatively slow at physiological pH in unbuffered aqueous solution due to the low concentration of the OH$^-$ ion catalyzing the exchange of the -NH protons [38]. On the other hand, such exchange can be promoted in the presence of buffer species through general base catalysis. [38,39] General base-catalyzed exchange pathway is expected to contribute to the overall relaxivity of the complex within the biologically relevant pH range (6–8). For this reason, the relaxivity of [Fe(CD2A-BA_2)]$^+$ was measured as a function of pH in both 50 mM HEPES and 50 mM piperazine buffer systems (Fig. S11). Equations and expressions used for the characterization of the exchange reactions between the -NH protons of Fe(CD2A-BA_2)]$^+$ and the bulk are reported in the ESI. The observed overall relaxation enhancement of [Fe(CD2A-BA_2)]$^+$ can be described by Eqs. S18, where the terms $^{FeL}r_{1pr}$ and $^{FeLH-1}r_{1pr}$ represent the contributions from prototropic exchange of the amide -NH protons in the FeL and FeLH$_{-1}$ species, respectively. According to the general theory of proton transfer, the process proceeds through the formation of a hydrogen-bonded adduct between the proton donor and acceptor. [40] In the case of base-catalyzed proton transfer, the rate of proton exchange (k_B and k_{HB}) is directly proportional to the difference in basicity between the donor and the acceptor. Based on the k_B value of piperazine, its proton exchange reaction is diffusion-controlled, owing to the significantly higher basicity of piperazine (logK_1 = 10.19 (2), logK_2 = 6.19 (3), 0.15 M $NaNO_3$, 25 °C) compared to that of the NH group in [Fe(CD2A-BA_2)]$^+$ (log$K_{MLH_{-2}}$= 9.2, Table 2). However, the k_{HB} value of the monoprotonated piperazine is approximately five orders of magnitude lower than k_B, which can be attributed to the lower basicity of its second nitrogen donor atom. Similarly, the deprotonated HEPES-assisted proton exchange (k_B) of the NH proton in [Fe(CD2A-BA_2)]$^+$ is about four orders of magnitude slower than that promoted by the deprotonated piperazine, reflecting the lower basicity of the nitrogen donor atom of HEPES (logK_1 = 7.30 (2), 0.15 M $NaNO_3$, 25 °C). It should be noted that the monoprotonated H-HEPES-assisted prototropic exchange of the amide -NH protons has a negligible contribution to the relaxation enhancement of the [Fe(CD2A-BA_2)]$^+$ complex. The longitudinal relaxation time (T_{1pr}) of the NH proton in [Fe(CD2A-BA_2)]$^+$ is 14 μs, which is roughly three times longer than that of the OH$^-$ proton in [Gd(HP-DO3A)] (Table 4). This difference is consistent with the larger Fe(III)–NH distance compared with the Gd(III)–OH distance. [38].

Relaxometric measurements as a function of both magnetic field strength and temperature were performed on the two butylamide complexes at pH values below the deprotonation threshold of the inner-sphere water molecule. The results are presented as Nuclear Magnetic Relaxation Dispersion (NMRD) profiles (Fig. 5), [41,42] which can provide valuable information on the water protons relaxation process in the investigated systems. The introduction of secondary amide groups on the CDTA scaffold not only imparts the structural features discussed above, but also markedly influences the molecular parameters governing relaxivity. In particular, the overall charge of the complexes is

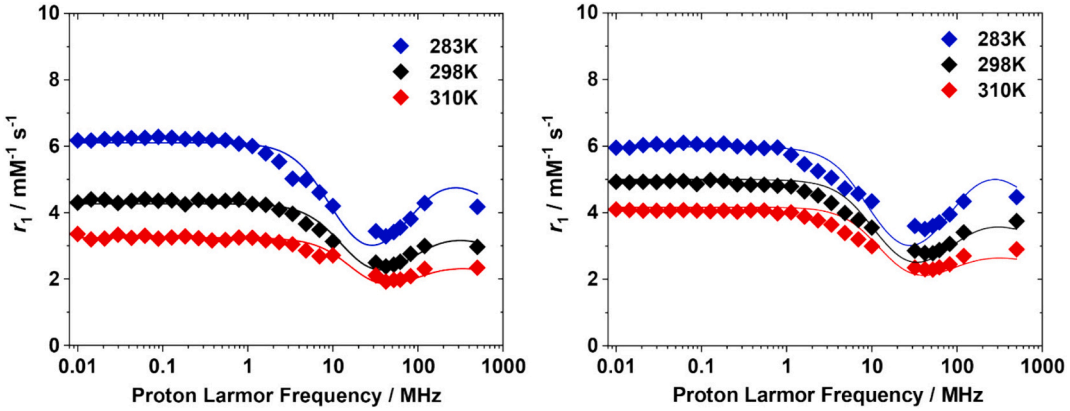

Fig. 5. ^{1}H NMRD profiles of Fe(III) complexes measured at different temperatures. (left) [Fe(CD3A-BA)] ([FeL] = 8.2 mM, pH = 6.0). (right) [Fe(CD2A-BA_2)]$^+$ ([FeL] = 4.2 mM, pH = 5.7).

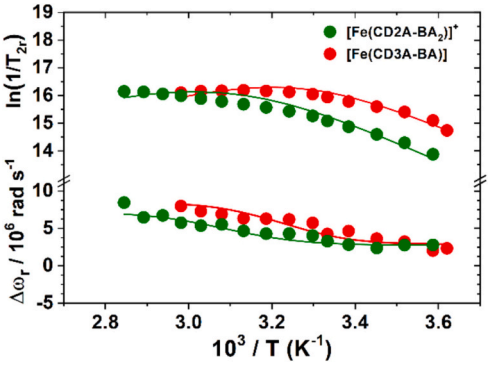

Fig. 6. Reduced ^{17}O NMR transverse relaxation rates (top) and chemical shifts (bottom) as a function of temperature for the Fe(III) complexes. ([Fe(CD3A-BA)] 3.8 mM, pH = 6.0; $[Fe(CD2A\text{-}BA_2)]^+$ 3.4 mM, pH = 5.7).

known to play a crucial role in determining the inner-sphere water exchange rate, [21,23,43] which can be reliably assessed by variable-temperature ^{17}O NMR measurements (Fig. 6). The relaxometric data were therefore interpreted through a global analysis of the ^{1}H NMRD and ^{17}O NMR datasets. Analysis of the ^{17}O NMR data was performed using the Swift–Connick equations, [44] while the ^{1}H NMRD profiles were fitted using the Solomon–Bloembergen–Morgan framework combined with the Freed model. [45–48] A summary of the optimized parameters is presented in Table 5, with the full dataset of fitted values reported in Table S2 of the ESI. Given the large number of variables involved in the fitting procedure, several parameters were fixed to known or literature values.

Given the structural similarities between $[Fe(CDTA)]^-$ and its mono- and bis-amide derivatives, a set of common assumptions was adopted: hydration number $q = 1$, Fe(III)–proton distance $r_{Fe-H} = 2.70$ Å, diffusion coefficients at 283, 298, and 310 K equal to $D = 1.30$, 2.24, and 3.10×10^{-5} cm^2 s^{-1}, respectively, activation energy for diffusion $E_D = 20.0$ kJ mol^{-1}, and a minimum solute–water distance for the outer-sphere mechanism of $a = 3.5$ Å. [23] These reasonable constraints enabled a consistent and straightforward interpretation of the experimental data. The inner-sphere water average lifetime (τ_M) and its activation enthalpy (ΔH_M), the rotational correlation time (τ_R) and its activation energy (E_R), as well as the scalar coupling constant ($A_{O/\hbar}$), were treated as adjustable parameters. In addition, the electron spin relaxation parameters - the mean-squared zero-field splitting energy (Δ^2) and its correlation time (τ_V) - were refined, while the activation energy for τ_V (E_V) was fixed at 1.0 kJ mol^{-1}. The obtained τ_R values are consistent with the molecular weights of the two butylamide complexes, showing the expected increase relative to the parent $[Fe(CDTA)]^-$ while remaining in excellent agreement with the corresponding mono- and bis-diethylamide derivatives of identical molecular weight. The electronic parameters Δ^2 and τ_V exhibit differences compared to the parent complex - an expected outcome of the modified coordination environment - yet they remain within the range observed for the DEA amides. [21] Likewise, the scalar coupling constant for the inner-sphere oxygen aligns well with values reported for other amide derivatives. A particularly noteworthy trend is the progressive slowing of the water exchange rate upon introduction of one or two amide groups into the CDTA scaffold. This behavior reflects the increased partial positive charge at the metal center, which strengthens the interaction with the oxygen atom of the inner-sphere water molecule. [43,49] Interestingly, comparison of the mono-butylamide complex with the mono-DEA analogue reported in the literature reveals a marked difference in residence time ($\tau_M = 65$ ns vs 110 ns, respectively), suggesting that steric effects from the amide substituent may modulate water exchange. When examining the bis-amide derivatives, the effect of steric hindrance becomes less evident and the partial positive charge on the metal center appears to play the predominant role in controlling the exchange dynamics. However, systems bearing substantially bulkier substituents demonstrate that steric effects can again become a decisive factor. This behavior is exemplified by the fluorinated $[Fe(CD2A2Am\text{-}CF_3Pip)]^+$ complex, a positively charged bis-amidic analogue in which the presence of a much larger substituent leads to an additional slowing of the water exchange rate. [24] Finally, to assess the actual efficiency of the Fe(III) complexes in generating contrast under physiologically relevant conditions, ^{1}H NMRD profiles were recorded in Seronorm®, a lyophilized human serum preparation that, once reconstituted, closely mimics physiological conditions, at 310 K. Comparison of the NMRD profiles obtained in aqueous solution and in this biological matrix provides valuable insight into possible interactions with serum proteins, transchelation events, or changes in the hydration state arising from the formation of ternary adducts. To probe these aspects, all measurements were performed at pH 6.0, where both complexes exist predominantly in their fully monohydrated form. The corresponding NMRD profiles are reported in the ESI (Fig. S12). Notably, the ^{1}H NMRD profiles recorded before and after the addition of serum were fully superimposable, indicating the absence of significant protein binding, no detectable Fe(III) demetallation or transchelation processes, and an unchanged hydration state. Furthermore, the r_1 values measured at 32 MHz and 310 K remained constant over the course of one week, providing additional confirmation of the long-term stability of the complexes under near-physiological conditions.

3.5. Cytotoxicity

Given the strong interest in developing alternatives to Gd(III)-based contrast agents, an increasing number of Fe(III)-based complexes [11,22,50] - and Fe-containing nanosystems- have recently been proposed as promising candidates. Several studies have even progressed to preliminary in vivo evaluations in murine models to explore their practical applicability. [12,51] However, in the development of any MRI contrast agent, the potential toxicity of the exogenous compound remains a critical parameter that must be rigorously assessed. Although some early toxicity data are available, [52,53] the rapid expansion of Fe-based MRI probes highlights the need for a more systematic characterization of their safety and biological behavior. In this rapidly evolving

Table 5
Selected parameters obtained from the simultaneous fit of ^{1}H NMRD profiles and ^{17}O NMR data.

	[Fe(CD3A-BA)]	$[Fe(CD2A\text{-}BA_2)]^+$	[Fe(CD3A-DEA)][a]	$[Fe(CD2A\text{-}DEA_2)]^+$[a]	$[Fe(CD2A2Am\text{-}CF_3Pip)]^+$[b]	[Fe(CDTA)][c]
$^{298}r_1$ 1.4 T / mM^{-1} s^{-1}	2.5	2.9	2.5	2.8	2.83	2.1
$^{298}\Delta^2$ / 10^{20} s^{-2}	13.5 (4)	11.3 (3)	12.6	11.9	10.5	18.1
$^{298}\tau_V$ / ps	3.8 (2)	3.5 (2)	4.3	3.8	4.2	3.4
$A_O/\hbar$ / 10^6 rad s^{-1}	−43.1 (3)	−35.6 (2)	−40.9	−34.6	−27	−62.8
$^{298}\tau_M^o$ / ns	65 (5)	218 (18)	110	222	526	36
ΔH_M / kJ mol^{-1}	52 (1)	54 (1)	52.0	56.0	38.9	51.5
$^{298}\tau_R$ / ps	56 (3)	69 (3)	58.0	66.0	66	48.4

[a] Ref [21].
[b] Ref [24].
[c] Ref [23].

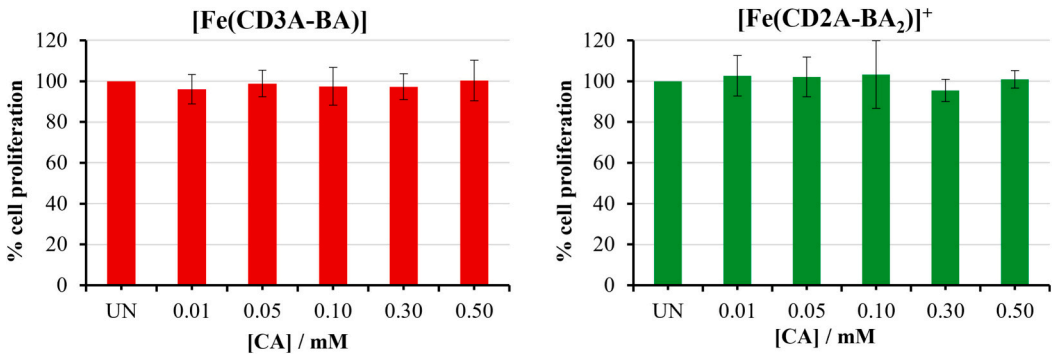

Fig. 7. Cell viability as a function of paramagnetic complex concentration. Data are represented as % of cell proliferation compared to untreated (UN) condition.

landscape, even individual contributions are valuable for building a reliable and comprehensive knowledge base. For this reason, cell viability assays were performed on HEK cell line (40,000 cells per well, DMEM medium) following a 24-*h* exposure to the two Fe(III) chelates. Cytotoxicity was assessed using the Sulforhodamine B (SRB) cytotoxicity assay, conducted on 4000 cells per well in 96-well plates. After cell fixation and staining with SRB, absorbance was measured at 565 nm. Reference compounds were analyzed in three biological replicates, each with three technical replicates while the Fe(III) complexes were evaluated across five independent biological replicates. As shown in Fig. 7, both Fe(III) complexes exhibited no detectable cytotoxicity under the experimental conditions, with cell viability remaining close to 100% even at concentrations as high as 0.5 mM after 24 *h* of incubation.

4. Conclusions

In this study, we investigated how the incorporation of one or two secondary butylamide substituents into the CDTA scaffold influences the structural and physicochemical properties of the corresponding Fe(III) complexes. These results were compared with the behavior previously reported for the analogous tertiary diethylamide (DEA) derivatives. The lower basicity of CD3A-BA and CD2A-BA$_2$ relative to CDTA leads to a pronounced decrease in the thermodynamic stability of their Fe(III) chelates. This destabilization is more significant than that observed for the DEA analogues, reflecting the weaker donor capacity of secondary amide oxygen atoms. Kinetic studies likewise reveal that substitution of carboxylate groups by secondary amides diminishes complex inertness: both butylamide complexes dissociate more rapidly than $[Fe(CDTA)]^-$ and the corresponding DEA derivatives, primarily via hydroxide-assisted pathways. These findings parallel the thermodynamic trends and support the established role of amide substitution in modulating Fe(III)–ligand interactions. Relaxometric ^{1}H NMRD and variable-temperature ^{17}O NMR measurements demonstrate that incorporation of neutral amide donors systematically slows inner-sphere water exchange as the overall complex charge becomes more positive. Although this effect follows the same general trend observed for the tertiary-amide series, the BA complexes exhibit shorter water residence times than their DEA counterparts with equivalent substitution levels, consistent with the distinct donor properties of secondary versus tertiary amides. Notably, in the bis-butylamide complex, the presence of a deprotonable amide –NH group introduces a prototropic exchange contribution within the physiological pH range - a feature absent in the tertiary-amide analogues. Under near-physiological conditions, both BA complexes remain monohydrated, show negligible protein binding or Fe(III) release in serum-like media, and display no detectable cytotoxicity in cell-viability assays.

Overall, the comparative analysis of secondary- and tertiary-amide CDTA derivatives confirms that amide substitution offers a powerful means of tuning the stability, kinetic inertness, and hydration dynamics of Fe(III)–CDTA complexes. The insights obtained from the butylamide series complement and extend those from the diethylamide derivatives, refining structure–property correlations that underpin the rational design of Fe(III)-based MRI contrast agents.

CRediT authorship contribution statement

M. Ludovica Macchia: Writing – original draft, Investigation, Data curation. **Marco Ricci:** Writing – original draft, Investigation, Data curation. **Mariangela Boccalon:** Investigation, Formal analysis. **Zsolt Baranyai:** Writing – original draft, Methodology, Data curation, Conceptualization. **Beatrice Ghezzi:** Writing – review & editing, Investigation. **Valentina Audrito:** Writing – review & editing, Formal analysis. **Mauro Botta:** Writing – review & editing, Methodology, Funding acquisition, Conceptualization.

Declaration of competing interest

The authors declare that they have no known competing financial interests or personal relationships that could have appeared to influence the work reported in this paper.

Acknowledgments

This manuscript is part of the project NODES which has received funding from the MUR-M4C2 1.5 of PNRR with grant agreement no. ECS00000036 (M. Botta, M.L.M.). M.R. acknowledge financial support from PRIN 2022 PNRR (PNRR M4C2, IDP20224R8YZ).

Appendix A. Supplementary data

Supplementary data to this article can be found online at https://doi.org/10.1016/j.jinorgbio.2026.113262.

Data availability

The authors declare that the data supporting the findings of this study are available within the article and its supplementary material. Raw data that support the findings of this study are available from the corresponding author, upon reasonable request.

References

[1] E. Kanal, Gadolinium based contrast agents (GBCA): *s*afety overview after 3 decades of clinical experience, Magn. Reson. Imaging 34 (10) (2016) 1341–1345, https://doi.org/10.1016/j.mri.2016.08.017.
[2] P. Caravan, Strategies for increasing the sensitivity of gadolinium based MRI contrast agents, Chem. Soc. Rev. 35 (6) (2006) 512–523, https://doi.org/10.1039/b510982p.
[3] K.B. Maier, L.N. Rust, F. Carniato, M. Botta, M. Woods, α-Aryl substituted GdDOTA derivatives, the perfect contrast agents for MRI? Chem. Commun. 60 (21) (2024) 2898–2901, https://doi.org/10.1039/d3cc05989h.
[4] Napolitano R., Guidolin N., Boccalon M., Fringuello Mingo A., Colombo Serra S., Buonsanti F., Fretta R., Demitri N., Bényei A., Botta M., Giovenzana G.B., Tedoldi

F., Baranyai Z., Chiral switch of gadopiclenol: new standards in MRI probes, *Adv. Sci.*, 2025, 12(14), 2415321, doi:https://doi.org/10.1002/advs.202415321.
[5] J.C. Bousquet, S. Saini, D.D. Stark, P.F. Hahn, M. Nigam, J. Wittenberg, J. T. Ferrucci, Gd-DOTA: characterization of a new paramagnetic complex, Radiology 166 (3) (1988) 693–698, https://doi.org/10.1148/radiology.166.3.3340763.
[6] L. Telgmann, M. Sperling, U. Karst, Determination of gadolinium-based MRI contrast agents in biological and environmental samples: *a* review, Anal. Chim. Acta 764 (2013) 1–16, https://doi.org/10.1016/j.aca.2012.12.007.
[7] J. Künnemeyer, L. Terborg, B. Meermann, C. Brauckmann, I. Möller, A. Scheffer, U. Karst, Speciation analysis of gadolinium chelates in hospital effluents and wastewater treatment plant sewage by a novel HILIC/ICP-MS method, Environ. Sci. Technol. 43 (8) (2009) 2884–2890, https://doi.org/10.1021/es803278n.
[8] K. Schmidt, M. Bau, G. Merschel, N. Tepe, Anthropogenic gadolinium in tap water and in tap water-based beverages from fast-food franchises in six major cities in Germany, Sci. Total Environ. 687 (2019) 1401–1408, https://doi.org/10.1016/j.scitotenv.2019.07.075.
[9] M. Botta, F. Carniato, D. Esteban-Gómez, C. Platas-Iglesias, L. Tei, Mn(II) compounds as an alternative to Gd-based MRI probes, Future Med. Chem. 11 (12) (2019) 1461–1483, https://doi.org/10.4155/fmc-2018-0608.
[10] P. Caravan, Divalent *m*anganese *c*omplexes as *p*otential *r*eplacements for *g*adolinium-*b*ased *c*ontrast *a*gents, Investig. Radiol. 59 (2) (2024) 187–196, https://doi.org/10.1097/rli.0000000000001053.
[11] E.A. Kras, E.M. Snyder, G.E. Sokolow, J.R. Morrow, Distinct *c*oordination *c*hemistry of Fe(III)-*b*ased MRI *p*robes, Acc. Chem. Res. 55 (10) (2022) 1435–1444, https://doi.org/10.1021/acs.accounts.2c00102.
[12] Snyder E.M., Asik D., Abozeid S.M., Burgio A., Bateman G., Turowski S.G., Spernyak J.A., Morrow J.R., A class of Fe III *m*acrocyclic complexes with *a*lcohol *d*onor groups as *e*ffective T1 MRI *c*ontrast *a*gents, *Angew. Chem.*, 2020, 132(6), 2435–2440, doi:https://doi.org/10.1002/ange.201912273.
[13] Uzal-Varela R., Lucio-Martínez F., Nucera A., Botta M., Esteban-Gómez D., Valencia L., Rodríguez-Rodríguez A., Platas-Iglesias C., A systematic investigation of the NMR relaxation properties of Fe(III)-EDTA derivatives and their potential as MRI contrast agents, *Inorg. Chem. Front.*, 2023, 10(5), 1633–1649, doi:https://doi.org/10.1039/d2qi02665a.
[14] E.A. Kras, R. Cineus, M.R. Crawley, J.R. Morrow, Macrocyclic complexes of Fe(iii) with mixed hydroxypropyl and phenolate or amide pendants as T1 MRI probes, Dalton Trans. 53 (9) (2024) 4154–4164, https://doi.org/10.1039/d3dt04013e.
[15] A. Gupta, P. Caravan, W.S. Price, C. Platas-Iglesias, E.M. Gale, Applications for *t*ransition-*m*etal chemistry in *c*ontrast-*e*nhanced *m*agnetic *r*esonance *i*maging, Inorg. Chem. 59 (10) (2020) 6648–6678, https://doi.org/10.1021/acs.inorgchem.0c00510.
[16] W.H. Koppenol, R.H. Hider, Iron and redox cycling. Do's and don'ts, Free Radic. Biol. Med. 133 (2019) 3–10, https://doi.org/10.1016/j.freeradbiomed.2018.09.022.
[17] H. Wang, V.C. Jordan, I.A. Ramsay, M. Sojoodi, B.C. Fuchs, K.K. Tanabe, P. Caravan, E.M. Gale, Molecular *m*agnetic *r*esonance *i*maging *u*sing a *r*edox-*a*ctive Iron *c*omplex, J. Am. Chem. Soc. 141 (14) (2019) 5916–5925, https://doi.org/10.1021/jacs.9b00603.
[18] P. Caravan, J.J. Ellison, T.J. McMurry, R.B. Lauffer, Gadolinium(III) chelates as MRI contrast agents: structure, dynamics, and applications, Chem. Rev. 99 (9) (1999) 2293–2352, https://doi.org/10.1021/cr980440x.
[19] G. González, D.H. Powell, V. Tissières, A.E. Merbach, Water-exchange, electronic relaxation, and rotational dynamics of the MRI contrast agent [Gd(DTPA-BMA)(H2O)] in aqueous solution: *a* variable pressure, temperature, and magnetic field 17O NMR study, J. Phys. Chem. 98 (1) (1994) 53–59, https://doi.org/10.1021/j100052a010.
[20] S. Aime, M. Botta, P.L. Anelli, F. Fedeli, M. Grandi, F. Uggeri, P. Paoli, Synthesis, *c*haracterization, and 1 /T1 NMRD *p*rofiles of gadolinium(III) complexes of *m*onoamide *d*erivatives of DOTA-*l*ike *l*igands. X-ray *s*tructure of the 10-[2-[[2-Hydroxy-1-(*h*ydroxymethyl)ethyl]amino]-1-[(Phenylmethoxy)*m*ethyl]-2-*o*xoethyl]-1, 4, 7, 10-*t*etra, Inorg. Chem. 31 (12) (1992) 2422–2428, https://doi.org/10.1021/ic00038a023.
[21] M.L. Macchia, A. Nucera, M. Ricci, F. Carniato, Z. Baranyai, M. Botta, Assessing the *i*mpact of *a*mide *d*onor *g*roups on *s*tability and NMR *r*elaxation *e*fficiency of *m*onohydrated Fe(III) *c*omplexes, Eur. J. Inorg. Chem. 27 (28) (2024) e202400341, https://doi.org/10.1002/ejic.202400341.
[22] J. Xie, A. Haeckel, R. Hauptmann, I.P. Ray, C. Limberg, N. Kulak, B. Hamm, E. Schellenberger, Iron(III)-tCDTA derivatives as MRI contrast agents: *i*ncreased T1 relaxivities at higher magnetic field strength and pH sensing, Magn. Reson. Med. 85 (6) (2021) 3370–3382, https://doi.org/10.1002/mrm.28664.
[23] Z. Baranyai, F. Carniato, A. Nucera, D. Horváth, L. Tei, C. Platas-Iglesias, M. Botta, Defining the conditions for the development of the emerging class of FeIII-based MRI contrast agents, Chem. Sci. 12 (33) (2021) 11138–11145, https://doi.org/10.1039/d1sc02200h.
[24] Z. Garda, F. Szeremeta, C.N. Tóth, S. Bunda, C. Pifferi, R. Clémençon, S. Même, G. Tircsó, É. Tóth, Relaxation-*b*ased *i*n *v*ivo *d*iscrimination of *o*xidized and *r*educed *s*tates of a *r*edox-*s*witchable 19F MRI *p*robe, J. Am. Chem. Soc. 147 (21) (2025) 18017–18024, https://doi.org/10.1021/jacs.5c03244.
[25] Lalli D., Ferrauto G., Terreno E., Carniato F., Botta M., Mn(ii)-Conjugated silica nanoparticles as potential MRI probes, *J. Mater. Chem. B*, 2021, 9(43), 8994–9004, doi:https://doi.org/10.1039/d1tb01600h.
[26] H.M. Irving, M.G. Miles, L.D. Pettit, A study of some problems in determining the stoicheiometric proton dissociation constants of complexes by potentiometric titrations using a glass electrode, Anal. Chim. Acta 38 (C) (1967) 475–488, https://doi.org/10.1016/s0003-2670(01)80616-4.
[27] L. Zekany, I. Nagypal, Psequad, computational *m*ethods for the *d*etermination of *f*ormation constants, springer, Boston, MA, 1985, pp. 291–353, https://doi.org/10.1007/978-1-4684-4934-1_8.
[28] H. Oe, N. Takahashi, E. Doi, M. Hirose, Effects of anion binding on the conformations of the two domains of ovotransferrin, J. Biochem. 106 (5) (1989) 858–863, https://doi.org/10.1093/oxfordjournals.jbchem.a122942.
[29] J.D. Carr, D.G. Swartzfager, Polarimetric studies of alkali metal ion complexes of I-frans-1,2-diaminocyclonexane-N,N,N′,N′-tetraaceuc acid, Anal. Chem. 43 (11) (1971) 1520–1522, https://doi.org/10.1021/ac60305a041.
[30] Sarka L., Bányai I., Brůcher E., Király R., Platzek J., Radüchel B., Schmitt-Willich H., Synthesis, equilibrium and NMR studies of lanthanide(m) complexes of the N-mono(niethylamide) and N′-mono(methylamide) derivatives of diethylenetriamine-N,N,N′,N″,N″-pentaacetic acid, *J. Chem. Soc. Dalton Trans.*, 2000, (20), 3699–3703, doi:https://doi.org/10.1039/b005298l.
[31] Z. Baranyai, Z. Pálinkás, F. Uggeri, E. Brücher, Equilibrium studies on the Gd3+, Cu2+ and Zn 2+ complexes of BOPTA, DTPA and DTPA-BMA ligands: *k*inetics of metal-exchange reactions of [Gd(BOPTA)]2, Eur. J. Inorg. Chem. 2010 (13) (2010) 1948–1956, https://doi.org/10.1002/ejic.200901261.
[32] Sarka L., Burai L., Király R., Zékány L., Brücher E., Studies on the kinetic stabilities of the Gd3+ complexes formed with the N-mono(methylamide), N′-mono(methylamide) and N,N″-bis(methylamide) derivatives of diethylenetriamine-N,N,N′,N″,N″-pentaacetic acid, *J. Inorg. Biochem.*, 2002, 91(1), 320–326, doi:https://doi.org/10.1016/s0162-0134(02)00418-x.
[33] J. Bloch, G. Navon, A nuclear magnetic resonance relaxation study of iron(III) EDTA in aqueous solution, J. Inorg. Nucl. Chem. 42 (5) (1980) 693–699, https://doi.org/10.1016/0022-1902(80)80215-6.
[34] Ma R., Motekaitis R.J., Martell A.E., Stability of metal ion complexes of N,N′-bis(2-hydroxybenzyl)ethylenediamine-N,N′-diacetic acid, *Inorg. Chim. Acta*, 1994, 224 (1–2), 151–155, doi:https://doi.org/10.1016/0020-1693(94)04012-5.
[35] Y. Li, B. Liu, Z. Ge, B. Yang, Spectroscopic analysis of the interaction between gallium(III) and apoovotransferrin, J. Photochem. Photobiol. B Biol. 91 (2–3) (2008) 137–142, https://doi.org/10.1016/j.jphotobiol.2008.03.001.
[36] G.W. Bates, M.R. Schlabach, The nonspecific binding of Fe3+ to transferrin in the absence of synergistic anions, J. Biol. Chem. 250 (6) (1975) 2177–2181, https://doi.org/10.1016/s0021-9258(19)41698-0.
[37] A. Nucera, M.L. Macchia, Z. Baranyai, F. Carniato, L. Tei, M. Ravera, M. Botta, Comprehensive *i*nvestigation of [Fe(EDTA)]−-*f*unctionalized *d*erivatives and their *s*upramolecular *a*dducts with *h*uman *s*erum *a*lbumin, Inorg. Chem. 63 (28) (2024) 12992–13004, https://doi.org/10.1021/acs.inorgchem.4c01715.
[38] S. Aime, S. Baroni, Castelli D. Delli, E. Brücher, I. Fábián, S.C. Serra, Mingo A. Fringuello, R. Napolitano, L. Lattuada, F. Tedoldi, Z. Baranyai, Exploiting the *p*roton *e*xchange as an *a*dditional *r*oute to *e*nhance the Relaxivity of *p*aramagnetic MRI *c*ontrast *a*gents, Inorg. Chem. 57 (9) (2018) 5567–5574, https://doi.org/10.1021/acs.inorgchem.8b00521.
[39] L. Leone, M. Boccalon, G. Ferrauto, I. Fábián, Z. Baranyai, L. Tei, Acid-catalyzed proton exchange as a novel approach for relaxivity enhancement in Gd-HPDO3A-like complexes, Chem. Sci. 11 (30) (2020) 7829–7835, https://doi.org/10.1039/d0sc02174a.
[40] M. Eigen, Proton *t*ransfer, Acid-Base *c*atalysis, and *e*nzymatic *h*ydrolysis. Part I: ELEMENTARY PROCESSES, Angew. Chem. Int. Ed. Eng. 3 (1) (1964) 1–19, https://doi.org/10.1002/anie.196400011.
[41] S. Aime, M. Botta, D. Esteban-Gómez, C. Platas-Iglesias, Characterisation of magnetic resonance imaging (MRI) contrast agents using NMR relaxometry, Mol. Phys. 117 (7–8) (2019) 898–909, https://doi.org/10.1080/00268976.2018.1516898.
[42] S.H. Koenig, R.D. Brown, Field-cycling relaxometry of protein solutions and tissue: *i*mplications for MRI, Prog. Nucl. Magn. Reson. Spectrosc. 22 (6) (1990) 487–567, https://doi.org/10.1016/0079-6565(90)80008-6.
[43] S. Laurent, L. Elst, Botteman F. Vander, R.N. Muller, An assessment of the potential relationship between the charge of Gd-DTPA complexes and the exchange rate of the water coordinated to the metal, Eur. J. Inorg. Chem. 2008 (28) (2008) 4369–4379, https://doi.org/10.1002/ejic.200800541.
[44] T.J. Swift, R.E. Connick, NMR-*r*elaxation mechanisms of O17 in aqueous solutions of paramagnetic cations and the lifetime of water molecules in the first coordination sphere, J. Chem. Phys. 37 (2) (1962) 307–320, https://doi.org/10.1063/1.1701321.
[45] L.P. Hwang, J.H. Freed, Dynamic effects of pair correlation functions on spin relaxation by translational diffusion in liquids, J. Chem. Phys. 63 (9) (1975) 4017–4025, https://doi.org/10.1063/1.431841.
[46] Freed J.H., Dynamic effects of pair correlation functions on spin relaxation by translational diffusion in liquids. II. Finite jumps and independent T 1 processes, *J. Chem. Phys.*, 1978, 68(9), 4034–4037, doi:https://doi.org/10.1063/1.436302.
[47] N. Bloembergen, L.O. Morgan, Proton relaxation times in paramagnetic solutions. Effects of electron spin relaxation, J. Chem. Phys. 34 (3) (1961) 842–850, https://doi.org/10.1063/1.1731684.
[48] I. Solomon, N. Bloembergen, Nuclear magnetic interactions in the HF molecule, J. Chem. Phys. 25 (2) (1956) 261–266, https://doi.org/10.1063/1.1742867.
[49] F. Carniato, M. Ricci, L. Tei, F. Garello, C. Furlan, E. Terreno, E. Ravera, G. Parigi, C. Luchinat, M. Botta, Novel *n*anogels *l*oaded with Mn(II) *c*helates as *e*ffective and *b*iologically *s*table MRI *p*robes, Small 19 (42) (2023) 2302868, https://doi.org/10.1002/smll.202302868.
[50] S. Chen, L. An, S. Yang, Low-*m*olecular-*w*eight Fe(III) *c*omplexes for MRI *c*ontrast *a*gents, Molecules 27 (14) (2022) 4573, https://doi.org/10.3390/molecules27144573.
[51] D. Asik, R. Smolinski, S.M. Abozeid, T.B. Mitchell, S.G. Turowski, J.A. Spernyak, J. R. Morrow, Modulating the properties of Fe(III) macrocyclic MRI contrast agents

by appending sulfonate or hydroxyl groups, Molecules 25 (10) (2020) 2291, https://doi.org/10.3390/molecules25102291.

[52] I.A. Rosales, I.Y. Zhou, I. Ay, M. Sojoodi, M.E. Sise, E.M. Gale, Imaging kidney inflammation using an oxidatively activated MRI probe, Kidney Int. 106 (4) (2024) 671–678, https://doi.org/10.1016/j.kint.2024.05.027.

[53] L. He, H. Wang, Z. Zeng, L. Zhong, Q. Tang, J. Yu, J. Tian, T. Liu, J. Zhu, Rigid Fe (III) chelate with *p*hosphonate *p*endants: *a* stable and *e*ffective *e*xtracellular MRI *c*ontrast *a*gent, J. Med. Chem. 67 (11) (2024) 8630–8641, https://doi.org/10.1021/acs.jmedchem.3c02338.